










High-temperature quantum coherence of spinons in a rare-earth spin chain

Lazar L. Kish ¹, Andreas Weichselbaum ¹, Daniel M. Pajerowski ², Andrei T. Savici ², Andrey Podlesnyak ², Leonid Vasylechko ³, Alexei Tsvelik ¹, Robert Konik ¹ and Igor A. Zaliznyak ^{1,*}

¹*Condensed Matter Physics and Materials Science Division,
Brookhaven National Laboratory, Upton, NY 11973, USA*

²*Neutron Scattering Division, Oak Ridge National Laboratory, Oak Ridge, TN 37831, USA*

³*Lviv Polytechnic National University, Lviv, Ukraine*

(Dated: June 25, 2024)

Although magnetism is a quantum phenomenon, its energy scale can be strong enough to sustain technological usage at room temperature and above. Temperature, however, leads to the decoherence which hampers quantum information applications. Common wisdom dictates that when magnets are heated to temperatures where thermal energy is higher than the interactions among atomic magnetic moments, the latter become uncorrelated and classical paramagnetic behavior is recovered. Surprisingly, our neutron scattering experiments on Yb chains in an insulating perovskite crystal overturn this conventional picture. We find a sharply defined spectrum of spinon excitations, which are the fractional elementary excitations in spin-1/2 chains, that persists to temperatures where thermal energy is more than 20 times higher than the energy of interactions between Yb magnetic moments, J . The observed sharpness of the spinon continuum boundary indicates that spinon mean free path exceeds ≈ 35 inter-atomic spacings at temperatures markedly above the magnetic energy scale. Our observations reveal an interesting and highly unusual quantum behavior in a rare earth magnet, which challenges quantum metrology and has profound implications for spin qubit systems in quantum information applications operating at finite temperatures.

One sentence summary: Our neutron scattering study reveals remarkable persistence of quantum coherence in an Yb qubit candidate spin chain at temperatures that exceed by more than an order of magnitude the energy scale of magnetic interactions governing its quantum dynamics.

Magnetism is the oldest quantum phenomenon, known for nearly 2500 years before it was understood following the discovery of electron spin [1] and the invention of quantum mechanics [2]. In addition to simple ferromagnetism, quantum theory predicts a great variety of other entangled spin states, such as in exactly solved antiferromagnetic spin-1/2 chains [3], where spins are entangled at all distances but have no static order. Consequently, spin systems are widely considered for quantum information applications requiring processing, transmission, and storage of entangled states. Quantum computation and communication algorithms using spin chains [4–8], fractional and topological excitations in quantum spin liquids [9–11], as well as magnons in ordered ferro- and antiferro-magnets [12–14] are being investigated.

The main hurdle for quantum computing applications is the decoherence of entangled states where unwanted interactions with the environment or excitations present at non-zero temperatures cause quantum information to be lost. The long-range coherence of quantum states present at $T = 0$ can be destroyed at $T > 0$ when excitations, such as magnons, change their identities by colliding and exchanging quantum numbers similarly to phonon-roton excitations in superfluid helium [15]. In a quantum spin-1 chain where the Haldane ground state is disordered, magnons separated from it by an energy gap, Δ_H , exhibit mesoscopic long-range coherence at $T = 0$, but the coherence is rapidly lost at temperatures $k_B T \sim \Delta_H$ (k_B is Boltzmann constant) as magnons become thermally excited [16–18]. The decoherence can be described as a finite collisional lifetime of magnon excitations encoding quantum states, which in this case can be accurately calculated [19]. Similarly, in ordered magnets magnons become over-damped at high temperatures, entirely losing their coherent quantum nature when temperature increases and thermal energy becomes comparable to magnon bandwidth [20, 21]. This thermal decoherence limits magnon potential for storage and transmission of quantum information.

Here, we find that the situation is entirely different for spinons, fractional excitations in a spin-1/2 chain, which retain quantum coherence up to temperatures where thermal energy exceeds characteristic energy scales of spin interactions by an order of magnitude, or more. Our magnetic inelastic neutron scattering (INS) measurements show that in the material realization of spin-1/2 chains in YbAlO_3 [22–24], the loss of quantum coherence stems from interactions with high-energy, thermal bath type degrees of freedom external to the effective spin Hamiltonian.

The magnetic doublets of rare earth Kramers ions such as Yb^{3+} in a crystal electric field (CEF) provide a fruitful approach to implementing quantum spin qubits in solids [25–28]. Although such

* zaliznyak@bnl.gov

a doublet has orbital character imposed by a strong spin-orbit coupling (SOC), it can be represented as a pseudo-spin-1/2, similar to the real spin-1/2 of an unpaired magnetic electron, implementing a quantum qubit. Advantageously, the states of a doublet can carry large angular momentum quantum numbers, which suppresses their interaction with magnetic fields of the environment by virtue of selection rules expressing angular momentum conservation [2]. Hence, such spin qubits can have longer coherence times [26, 27]. Such is the situation of Yb^{3+} ions in a perovskite, YbAlO_3 [22–24], which we study here. Strong SOC (one of the strongest among all lanthanides) combines the spin ($S = 1/2$) and the orbital ($L = 3$) angular momenta of a single hole in the $4f$ shell of Yb^{3+} into a total angular momentum \mathbf{J} ($J = 7/2$), effectively quenching the spin degree of freedom by rigidly tying it to the dominant orbital contribution. This leads to a very simple electronic level structure, which is within the reach of near-infrared or visible photons. Consequently, Yb atoms make world’s most accurate atomic clocks, highly efficient high-power crystal and fiber lasers, and optical amplifiers, holding the record for femtosecond pulses with highest average power, and are a promising system for optically controlled quantum information applications [26]. A chain of coupled Yb spins (doublets) implements a chain of coupled qubits where coherently propagating spinon excitations act to switch the state of each qubit.

Spin-1/2 chains are often encountered in magnetic crystals and have been studied extensively in the literature [29–31]. However, to our knowledge the important question of what happens to spinon excitations with increasing temperature remains experimentally unexplored, mainly because the exchange energy scales in most studied spin-chain materials are in the range of tens to hundreds of meV ($J/k_B \sim 100 - 1000$ K, k_B is Boltzmann constant), which makes it difficult to reach temperatures in true excess of the excitation energy. From this perspective, YbAlO_3 is an ideal material to study as exchange interaction in its effective spin-1/2 Hamiltonian is relatively weak ($J \approx 0.21$ meV, $J/k_B \approx 2.4$ K [23, 24]) and it does not order down to a temperature of 0.8 K. As a result, we can use inelastic neutron spectroscopy to probe the physics of the Heisenberg spin-1/2 chain in a temperature regime that is unattainable in other spin-1/2 chain materials.

Here, we report a detailed INS investigation of the spinon spectrum in YbAlO_3 as a function of temperature in 2 – 100 K ($\sim (1 - 40) \times J$) range. As is well known, the excitation spectrum of the ideal spin-1/2 Heisenberg chain is formed by pairs of spinons, fractional elementary excitations each carrying $S = 1/2$ angular momentum [3]. Pair-states of these spinon excitations encode physical spin flips in the chain, whose energy spectrum forms a continuum, at zero-temperature

sharply bounded by the two-spinon boundaries (q is wave vector, d is lattice spacing) [29–32],

$$\frac{\pi}{2}J|\sin qd| \leq \epsilon(q) \leq \pi J \left| \sin \left(\frac{qd}{2} \right) \right| \quad (1)$$

Qualitatively, the lower and upper two-spinon continuum boundaries show different behavior as a function of temperature, which can be understood by considering spinons as fermion quasiparticles half-filling the one-dimensional energy band, $\epsilon(q) = \frac{\pi}{2}J \sin qd$ [33]. The lower continuum boundary arises because of complete occupation of states below the spinon Fermi energy at zero temperature, which forbids excitations into the filled states. With the increasing temperature, the Fermi distribution smears out allowing state occupations above the Fermi level at the expense of the occupied states below it. As a result, the lower boundary gets smeared until it completely disappears at temperatures $\gtrsim \frac{\pi}{2}J/k_B$. On the other hand, the upper boundary reflects the maximum energy that a spinon pair with a given q can have according to the dispersion, $\epsilon(q)$. In the absence of spinon decoherence through finite collisional lifetime in an idealized system described by the quantum spin-chain Hamiltonian, the profile of the upper two-spinon boundary must remain completely untouched by temperature effects. The upper boundary of the excitation continuum is only blurred beyond the two-spinon boundary by the presence of multi-spinon-excitations, which at $T = 0$ amount to only a small, $\sim 1\%$ contribution above it [32]. While this blurring is in fact temperature-dependent, it is entirely governed by the quantum spin Hamiltonian and as our theoretical calculations show remains insignificant even at high temperatures, $T \gg J/k_B$.

In the presence of coupling to a system external to the quantum spin Hamiltonian, such as a thermal heat bath or other extrinsic source of decoherence, a quantum spin-chain will experience information loss to these external degrees of freedom. This will be reflected by a reduced spinon lifetime, measurable in neutron spectra by a broadening along the energy direction above instrument resolution. A blurring of the upper boundary of the excitation continuum in excess of the theoretically calculated width generated by multi-spinon excitations is then a metric for spinon decoherence, quantifying the degree of information loss from the spin-chain to the environment.

Figure 1 shows the temperature dependence of the measured spinon continuum in YbAlO_3 side-by-side with temperature-dependent realizations of the spin-1/2 Heisenberg model from finite-temperature DMRG calculations (see Methods). The left column shows our experimentally measured dynamical structure factors, normalized to absolute units as described in the Supplementary Information [34]. The middle column shows a fit of our DMRG-calculated spectrum to the experimental data, including convolution with the known instrumental resolution function and

a Lorentzian broadening function with half-width Γ to model finite spinon life-time, $\tau = \hbar/\Gamma$ [15, 16]. The right column shows the DMRG calculations without the Lorentzian broadening, demonstrating how the spectrum would appear if the effects of spinon thermal decoherence were absent. The waterfall plot in Fig. 2 shows constant- L line-cuts of data and the corresponding Lorentzian-broadened DMRG calculation at selected wave-vectors, which demonstrates the excellent agreement between our model and data (values for the reduced χ^2 goodness-of-fit parameter are listed in the caption and are below 3 for all temperatures; L is the component of the wave vector, $Q = (H, K, L)$, along the chain direction, see Methods).

At 2 K, the lower continuum boundary is visible in both experiment and DMRG simulations, albeit already slightly blurred by thermal repopulation as temperature is comparable to the exchange coupling, $J/k_B = 2.4$ K. At higher temperatures, 10 K and above, all signs of the lower continuum boundary have disappeared in both experiment and simulation and instead been replaced by a flat continuum. This flat continuum, however, remains clearly bounded by the dispersive upper boundary even at temperatures far higher than the exchange coupling. Remarkably, our experimentally measured datasets demonstrate this clear upper-boundary dispersion at temperatures as high as 100 K, forty times greater than the exchange interactions within the system. Only a slight blurring of the upper boundary can be seen, which is most clearly visible in the 1-dimensional plots in Fig. 2. This blurring appears well modelled by the wave-vector-independent Lorentzian damping, Γ , indicating finite spinon lifetime at high temperatures.

Figure 3 (A) shows Γ as a function of temperature, revealing no measurable spectral broadening beyond resolution at temperatures below 60 K. Above this point, however, the dispersion does become measurably blurred, with Γ eventually reaching an energy-scale of ~ 0.1 meV at 100 K, consistent with thermally activated behavior. An Arrhenius type fit, $\Gamma(T) = \Gamma_0 e^{-\frac{E_a}{k_B T}}$, yields activation energy, $E_a \approx 20$ meV. This energy scale is consistent with thermal population of crystal-field levels other than the ground-state doublet, which invalidates the $S_{eff} = 1/2$ description of the Yb ions, leading to information loss.

Using the group velocity of spinons from the dispersion near $L = 0$, $v = \pi J/2$, we can obtain an effective spinon coherence length (mean free path), $\xi = v\tau = v\hbar/\Gamma$, shown in Figure 3 (B) versus the reciprocal of temperature. When measurable broadening does develop at temperatures above 60 K, the effective coherence length appears to track a decreasing exponential trend with increasing temperature. Fits to an Arrhenius-type model, $\xi = \xi_0 e^{\frac{E_a}{k_B T}}$, where values $\xi > \xi_0$ are replaced by the fit constant $\xi_0 \approx 35$ corresponding to our resolution limit, are shown over-plotted

on the measured data in Figure 3 (B). According to this analysis, the coherence length exceeds 35 lattice units as it passes beyond the resolution limit of our measurements at staggeringly high temperature of 40 K ($\approx 17J$). The value of $E_a \approx 20$ meV obtained through this analysis is close to values for the CEF splitting reported in the literature [23]. Thus, the major spin-decoherence mechanism at play is likely to be thermal excitation of crystal-field levels outside the $S_{\text{eff}} = 1/2$ doublet, which presents defects in the chain that are able to change the number of spinons in the system on measurable timescales.

The coherence length encoded in the spinon lifetime ($\xi > 12$ nm) is comparable to the mesoscopic quantum coherence length of Haldane gap magnons observed near zero temperature in spin-1 chains [17]. There, however, excitation coherence is quickly lost with the increasing temperature due to collisions that change the quasiparticle content of the excited states and therefore limit the quasiparticle lifetime [17–19]. Consequently, magnons become over-damped at temperatures where thermal energy becomes comparable to the energy of spin interactions. Remarkably, this collisional lifetime mechanism is absent in the case of spinons in the spin-1/2 chain as spinons retain their intrinsic coherence at temperatures much higher than those characteristic of spin Hamiltonian.

It is of interest to put our results in the context of quantum metrology, which allows calculating model-independent quantities called entanglement witnesses that can be used to place bounds on the degrees of multipartite quantum entanglement present in the system [35, 36]. Of specific relevance is the quantum Fisher information (QFI), $F_Q(\hat{A})$ [37], a quantity that can be defined at finite temperature for any system through an imaginary part of dynamical susceptibility with respect to a variable, \hat{A} , in that system, $\chi''_A(E)$,

$$F_Q(\hat{A}) = \frac{1}{4\pi} \int_0^\infty dE \tanh\left(\frac{E}{2k_B T}\right) \chi''_A(E) \quad (2)$$

For spin-1/2 chain, the QFI, F_Q , can be obtained for $\hat{A} = \hat{S}^z$ from dynamical spin susceptibility at any wave-vector, $\chi''(Q, E)$. Equivalently, it can be obtained from the dynamical spin structure factor, $S(Q, E)$, measured by INS (Fig. 1), which is related to $\chi''(Q, E)$ via fluctuation-dissipation theorem [16, 35, 36]. The obtained QFI can then be used to place lower limits on the level of multipartite entanglement in the system, where QFI $F_Q > n$ at a certain wave vector imply at least $(n + 1)$ -partite entanglement in the system (Kramers-Rao bound) [35–37].

Figure 3 (C) shows the wave-vector-dependent QFI calculated from our neutron spectra for temperatures down to 80 mK (open circles), as well as from our idealized DMRG model (solid

curves). The dashed curve represents an approximation to the theoretical maximum at zero temperature, $F_Q|_{T=0} = 4S(Q)$ [38], where $S(Q) = \int_{-\infty}^{\infty} S(Q, E)dE$ is static structure factor given by Fourier transform of the single-time two-point spin correlation function, obtained from DMRG calculations at 200 mK ($\approx 0.01J/k_B T$). The temperature dependence of the maximum quantum Fisher information $F_Q(L = 1)$ is shown in Figure 3 (D) with power-law fits to the asymptotic behavior for both experiment and the idealized DMRG model. Our analysis shows excellent agreement between DMRG and neutron scattering measurements at all temperatures above the magnetic ordering transition, $T_N \approx 0.8$ K. At very low temperatures, F_Q in the idealized model continues to rise, demonstrating at least quadpartite entanglement at 200 mK. In contrast, in YbAlO_3 the QFI is arrested with $F_Q \approx 1$ at T_N , though enough spectral weight remains at high energy for it to demonstrate at least bipartite entanglement.

At high-temperature, $F_Q(L = 1)$ exhibits a near-perfect T^{-2} power-law decay for both experiment and theory. As it decays below a value 1 usable for a Kramers-Rao lower bound already at $T \gtrsim 0.5J/k_B$, F_Q does not provide a useful metric for quantum coherence that might be present in the system at high temperature, such as would describe the lifetime or mean free path of a spinon excitation. This poses a challenge of developing novel quantum metrology to capture high-temperature quantum behaviors in integrable systems, perhaps based on entanglement entropy, negativity, or some other concepts.

The observed long-range dynamical coherence associated with propagating spinons also contrasts sharply with the local character of single-time two-spin correlation function, $\langle S_j^z S_{j'}^z \rangle \approx 1/4\delta_{jj'}$ ($\delta_{jj'}$ is Kronecker delta), at $T \gg J/k_B$ and classical expectation of non-propagative, over-damped or diffusive dynamics in this regime [39]. Like QFI, the single-time correlation is insensitive to dynamical coherence because it encodes an energy-integrated property, static structure factor, $S(Q)$. At high temperature, $S(Q) \approx 1/4$ is Q -independent, indicating vanishing single-time spin-spin correlations.

The time-dependent, dynamical correlations revealing spinon coherence can be visualized by Fourier transforming the measured $\chi''(Q, E)$ to describe the real-space linear response, $\chi''(x, t)$ [40]. This is shown in Figure 4 as a sequence of color-plots scaled by the thermal factor T/J , where panels (A-D) show Fourier-transformed (FT) inelastic neutron data, (E-H) show the corresponding Fourier-transforms of our fits to the data, and (I-L) show the space-time theoretical DMRG data. While for $t = 0$ $\chi''(x, t)$ is only non-zero at the origin, $x = 0$, consistent with local single-time correlation, the $t > 0$ dynamics at all temperatures are governed by a clearly defined,

coherent “light cone” bounded by the spinon velocity. This light cone feature corresponds in the wave-vector-energy domain to the dispersive upper boundary of the spinon spectrum, and its presence at high temperatures testifies to the coherent nature of excitations. Remarkably, the linear ballistic transport regime appears to persist at short times even when thermal energy scale markedly exceeds interactions. At long times, however, the transport appears to cross over into a super-diffusive regime, $x \sim t^{2/3}$. Such a super-diffusive regime is predicted in the high-temperature limit of the Heisenberg chain and has been of interest for some number of years, but to our knowledge this is the clearest experimental demonstration of such a behavior to date [41]. At very high temperatures, experiment and fits experience a Lorentzian broadening along the energy axis, which indicates a shortening of the coherence time and a faster decay of time correlations absent in the purely theoretical model, Fig. 4 (I-L).

Topologically-protected spinon excitations in integrable systems present an attractive avenue towards encoding information in the spin degree of freedom in materials. Our work demonstrates remarkable quantum coherent behavior of spinons hosted by the effective $S = 1/2$ Heisenberg chains in YbAlO_3 , including ballistic and super-diffusive propagation at temperatures far exceeding the energy-scales at which individual spins interact with each other. The lifetime of these excitations remains longer than our experimental resolution up to very high temperatures, comparable to the crystal-field levels splitting of the Yb^{3+} ions, whose thermal population destabilizes the ground-state Kramers doublets underlying the spin-1/2 Heisenberg chain physics. In turn, this provides a possible control mechanism for the quantum-collective behaviors in optically-active rare-earth chains where optically-excited ions can be used to control the propagation of information [25]. Overall, our results suggest that such integrable rare-earth spin-systems may have a far broader range of quantum information applications than previously realized and also challenge quantum metrology to develop new methods suitable for gauging high-temperature dynamical coherence in quantum systems.

Methods:

Neutron scattering. The time-of-flight neutron scattering measurements were performed at the Cold Neutron Chopper Spectrometer (CNCS), Spallation Neutron Source (SNS). $E_i = 1.55$ meV ($\lambda = 7.26$ Å) was used. Here, chopper resolution settings resulted in a resolution full-width-half-maximum (FWHM) of 0.038 meV at the elastic position [see dashed line in Fig. 3 (A)]. A single crystal sample of YbAlO_3 [23] was mounted with its orthorhombic \mathbf{a} direction vertical, which allowed spectral mapping in the $(0, K, L)$ scattering plane. The wave vector, $Q = (H, K, L)$, is

measured in reciprocal lattice units of the orthorhombic $Pbnm$ lattice of YbAlO_3 ($a = 5.126 \text{ \AA}$, $b = 5.331 \text{ \AA}$, and $c = 7.313 \text{ \AA}$), where Yb-Yb spacing along the chain direction is $d = c/2$. Neutron intensities were binned on a uniform grid in wave-vector and energy, with a focus on two-dimensional slices in the $L - E$ plane. Details of the analyses including fitting to numerical models are described in the Supplementary Information [34].

Finite-temperature DMRG calculations. The dynamical structure factor (DSF) $S_{\text{DMRG}}(q, E)$ vs. one-dimensional in-chain momentum $q \equiv L/2$ and energy E was computed within DMRG in real-time and real-frequency from the retarded correlation function,

$$S^{\text{ret}}(x, t) \equiv -i\vartheta(t) \langle \hat{S}_x(t) \hat{S}_0^\dagger \rangle_T, \quad (3)$$

where $\hat{S}_x(t) \equiv e^{i\hat{H}t} \hat{S}_x e^{-i\hat{H}t}$ is the spin operator \hat{S} acting on site x at time t in the Heisenberg picture, with \hat{H} the Hamiltonian. Since DMRG operates on a finite system of length $N = 64$ with open boundary conditions (BCs) and lattice constant $d := 1$, the DSF was computed relative to the system center, referred to as origin ‘0’ above, hence having integer $x \in [-N/2 + 1, N/2]$. The time evolution was considered up until the light cone was about to reach the open system boundary. This data was then zero-padded towards larger system $|x| > N/2$ and extended in time via linear prediction, followed by double Fourier transform to momentum q and energy E . Additional details are presented in the Supplementary Information [34].

Acknowledgments We are grateful to the SNS staff for invaluable technical assistance and to C. Broholm, M. Mourigal, and A. Zheludev for valuable discussions. The work at Brookhaven National Laboratory was supported by Office of Basic Energy Sciences (BES), Division of Materials Sciences and Engineering, U.S. Department of Energy (DOE), under contract DE-SC0012704. This research used resources at the Spallation Neutron Source, a DOE Office of Science User Facility operated by Oak Ridge National Laboratory.

Author contributions: I.Z. conceived and directed the study. L.K., I.Z., D.P., A.P. and A.S. carried out neutron scattering experiments and obtained the data. L.K. performed fitting of the neutron spectra. L.K. and I.Z. analyzed the data and prepared the figures. A. W. performed theoretical DMRG calculations. R. K. and A. T. carried out theoretical analyses. L.V. provided the single crystals used in this study. I.Z. and L.K. wrote the paper, with input from all authors. **Competing Interests:** The authors declare that they have no competing interests. **Data availability:** All data needed to evaluate the conclusions in the paper are present in the paper and/or the Supplementary Materials. Additional data available from authors upon reasonable request.

-
- [1] G. E. Uhlenbeck and S. Goudsmit, Spinning Electrons and the Structure of Spectra, *Nature* **117**, 264 (1926).
- [2] P. A. M. Dirac, *The Principles of Quantum Mechanics*, International Series of Monographs on Physics (Clarendon Press, 1930, 4th ed. 1981).
- [3] H. Bethe, Zur Theorie der Metalle: I. Eigenwerte und Eigenfunktionen der linearen Atomkette, *Zeitschrift für Physik* **71**, 205 (1931).
- [4] S. Bose, Quantum communication through an unmodulated spin chain, *Physical Review Letters* **91**, 207901 (2003).
- [5] L. C. Venuti, C. D. E. Boschi, and M. Roncaglia, Qubit teleportation and transfer across antiferromagnetic spin chains, *Physical Review Letters* **99**, 060401 (2007).
- [6] Y. Tserkovnyak and D. Loss, Universal quantum computation with ordered spin-chain networks, *Physical Review A* **84**, 032333 (2011).
- [7] O. V. Marchukov, A. G. Volosniev, M. Valiente, D. Petrosyan, and N. T. Zinner, Quantum spin transistor with a Heisenberg spin chain, *Nature Communications* **7**, 10.1038/ncomms13070 (2016).
- [8] K. F. Thompson, C. Gokler, S. Lloyd, and P. W. Shor, Time independent universal computing with spin chains: quantum plinko machine, *New Journal of Physics* **18**, 073044 (2016).
- [9] A. Y. Kitaev, Fault-tolerant quantum computation by anyons, *Annals of Physics* **303**, 2 (2003).
- [10] C. Broholm, R. J. Cava, S. A. Kivelson, D. G. Nocera, M. R. Norman, and T. Senthil, Quantum spin liquids, *Science* **367**, 10.1126/science.aay0668 (2020).
- [11] G. Semeghini, H. Levine, A. Keesling, S. Ebadi, T. T. Wang, D. Bluvstein, R. Verresen, H. Pichler, M. Kalinowski, R. Samajdar, A. Omran, S. Sachdev, A. Vishwanath, M. Greiner, V. Vuletić, and M. D. Lukin, Probing topological spin liquids on a programmable quantum simulator, *Science* **374**, 1242 (2021).
- [12] P. Andrich, C. F. de las Casas, X. Liu, H. L. Bretscher, J. R. Berman, F. J. Heremans, P. F. Nealey, and D. D. Awschalom, Long-range spin wave mediated control of defect qubits in nanodiamonds, *npj Quantum Information* **3**, 10.1038/s41534-017-0029-z (2017).
- [13] D. Lachance-Quirion, Y. Tabuchi, A. Gloppe, K. Usami, and Y. Nakamura, Hybrid quantum systems based on magnonics, *Applied Physics Express* **12**, 070101 (2019).
- [14] A. V. Chumak, P. Kabos, M. Wu, C. Abert, C. Adelman, A. O. Adeyeye, J. Åkerman, F. G. Aliev,

- A. Anane, A. Awad, C. H. Back, A. Barman, G. E. W. Bauer, M. Becherer, E. N. Beginin, V. A. S. V. Bittencourt, Y. M. Blanter, P. Bortolotti, I. Boventer, D. A. Bozhko, S. A. Bunyaev, J. J. Carmiggelt, R. R. Cheenikundil, F. Ciubotaru, S. Cotofana, G. Csaba, O. V. Dobrovolskiy, C. Dubs, M. Elyasi, K. G. Fripp, H. Fulara, I. A. Golovchanskiy, C. Gonzalez-Ballester, P. Graczyk, D. Grundler, P. Gruszecki, G. Gubbiotti, K. Guslienko, A. Haldar, S. Hamdioui, R. Hertel, B. Hillebrands, T. Hioki, A. Houshang, C.-M. Hu, H. Huebl, M. Huth, E. Iacocca, M. B. Jungfleisch, G. N. Kakazei, A. Khitun, R. Khymyn, T. Kikkawa, M. Kläui, O. Klein, J. W. Kłos, S. Knauer, S. Koraltan, M. Kostylev, M. Krawczyk, I. N. Krivorotov, V. V. Kruglyak, D. Lachance-Quirion, S. Ladak, R. Lebrun, Y. Li, M. Lindner, R. Macêdo, S. Mayr, G. A. Melkov, S. Mieszczak, Y. Nakamura, H. T. Nembach, A. A. Nikitin, S. A. Nikitov, V. Novosad, J. A. Otálora, Y. Otani, A. Papp, B. Pigeau, P. Pirro, W. Prod, F. Porrati, H. Qin, B. Rana, T. Reimann, F. Riente, O. Romero-Isart, A. Ross, A. V. Sadovnikov, A. R. Safin, E. Saitoh, G. Schmidt, H. Schultheiss, K. Schultheiss, A. A. Serga, S. Sharma, J. M. Shaw, D. Suess, O. Surzhenko, K. Szulc, T. Taniguchi, M. Urbánek, K. Usami, A. B. Ustinov, T. van der Sar, S. van Dijken, V. I. Vasyuchka, R. Verba, S. V. Kusminskiy, Q. Wang, M. Weides, M. Weiler, S. Wintz, S. P. Wolski, and X. Zhang, Advances in magnetics roadmap on spin-wave computing, *IEEE Transactions on Magnetism* **58**, 1 (2022).
- [15] M. D. Nichitiu, C. Brown, and I. A. Zaliznyak, Breakdown of sound in superfluid helium, *Physical Review B* **109**, 1060502 (2024).
- [16] I. A. Zaliznyak, L.-P. Regnault, and D. Petitgrand, Neutron-scattering study of the dynamic spin correlations in CsNiCl₃ above Néel ordering, *Physical Review B* **50**, 15824 (1994).
- [17] G. Xu, C. Broholm, Y.-A. Soh, G. Aeppli, J. F. DiTusa, Y. Chen, M. Kenzelmann, C. D. Frost, T. Ito, K. Oka, and H. Takagi, Mesoscopic Phase Coherence in a Quantum Spin Fluid, *Science* **317**, 1049 (2007).
- [18] A. Zheludev, V. O. Garlea, L.-P. Regnault, H. Manaka, A. Tsvetlik, and J.-H. Chung, Extended Universal Finite-T Renormalization of Excitations in a Class of One-Dimensional Quantum Magnets, *Physical Review Letters* **100**, 157204 (2008).
- [19] S. Sachdev and K. Damle, Low Temperature Spin Diffusion in the One-Dimensional Quantum O(3) Nonlinear σ Model, *Physical Review Letters* **78**, 943 (1997).
- [20] T. Huberman, D. A. Tennant, R. A. Cowley, R. Coldea, and C. D. Frost, A study of the quantum classical crossover in the spin dynamics of the 2DS= 5/2 antiferromagnet Rb₂MnF₄: neutron scattering, computer simulations and analytic theories, *Journal of Statistical Mechanics: Theory and Experiment*

- 2008**, P05017 (2008).
- [21] S. P. Bayrakci, D. A. Tennant, P. Leininger, T. Keller, M. C. R. Gibson, S. D. Wilson, R. J. Birgeneau, and B. Keimer, Lifetimes of antiferromagnetic magnons in two and three dimensions: Experiment, theory, and numerics, *Physical Review Letters* **111**, 017204 (2013).
- [22] L. S. Wu, S. E. Nikitin, M. Brando, L. Vasylechko, G. Ehlers, M. Frontzek, A. T. Savici, G. Sala, A. D. Christianson, M. D. Lumsden, and A. Podlesnyak, Antiferromagnetic ordering and dipolar interactions of YbAlO_3 , *Physical Review B* **99**, 195117 (2019).
- [23] L. S. Wu, S. E. Nikitin, Z. Wang, W. Zhu, C. D. Batista, A. M. Tsvelik, A. M. Samarakoon, D. A. Tennant, M. Brando, L. Vasylechko, M. Frontzek, A. T. Savici, G. Sala, G. Ehlers, A. D. Christianson, M. D. Lumsden, and A. Podlesnyak, Tomonaga-Luttinger liquid behavior and spinon confinement in YbAlO_3 , *Nature Communications* **10**, 698 (2019).
- [24] S. E. Nikitin, T. Xie, A. Podlesnyak, and I. A. Zaliznyak, Experimental observation of magnetic dimers in diluted Yb:YAlO_3 , *Physical Review B* **101**, 245150 (2020).
- [25] D. D. Awschalom, R. Hanson, J. Wrachtrup, and B. B. Zhou, Quantum technologies with optically interfaced solid-state spins, *Nature Photonics* **12**, 516 (2018).
- [26] T. Zhong, J. M. Kindem, J. G. Bartholomew, J. Rochman, I. Craiciu, E. Miyazono, M. Bettinelli, E. Cavalli, V. Verma, S. W. Nam, F. Marsili, M. D. Shaw, A. D. Beyer, and A. Faraon, Nanophotonic rare-earth quantum memory with optically controlled retrieval, *Science* **357**, 1392 (2017), <https://science.sciencemag.org/content/357/6358/1392.full.pdf>.
- [27] A. Ruskuc, C.-J. Wu, J. Rochman, J. Choi, and A. Faraon, Nuclear spin-wave quantum register for a solid-state qubit, *Nature* **602**, 408 (2022).
- [28] A. Beckert, M. Grimm, N. Wili, R. Tschaggelar, G. Jeschke, G. Matmon, S. Gerber, M. Müller, and G. Aeppli, Emergence of highly coherent two-level systems in a noisy and dense quantum network, *Nature Physics* 10.1038/s41567-023-02321-y (2024).
- [29] B. Lake, D. A. Tennant, C. D. Frost, and S. E. Nagler, Quantum criticality and universal scaling of a quantum antiferromagnet, *Nature Materials* **4**, 329 (2005).
- [30] I. A. Zaliznyak, H. Woo, T. G. Perring, C. L. Broholm, C. D. Frost, and H. Takagi, Spinons in the Strongly Correlated Copper Oxide Chains in SrCuO_2 , *Physical Review Letters* **93**, 087202 (2004).
- [31] M. Mourigal, M. Enderle, A. Klöpperpieper, J.-S. Caux, A. Stunault, and H. M. Rønnow, Fractional spinon excitations in the quantum heisenberg antiferromagnetic chain, *Nature Physics* **9**, 435 (2013).
- [32] J.-S. Caux and R. Hagemans, The four-spinon dynamical structure factor of the Heisenberg chain,

- Journal of Statistical Mechanics: Theory and Experiment **2006**, P12013 (2006).
- [33] W. J. Gannon, I. A. Zaliznyak, L. S. Wu, A. E. Feiguin, A. M. Tsvelik, F. Demmel, Y. Qiu, J. R. D. Copley, M. S. Kim, and M. C. Aronson, Spinon confinement and a sharp longitudinal mode in $\text{Yb}_2\text{Pt}_2\text{2Pb}$ in magnetic fields, *Nature Communications* **10**, 1123 (2019).
- [34] See supplementary information for details of data and theoretical analysis and dmrg calculations.
- [35] A. Scheie, P. Laurell, A. M. Samarakoon, B. Lake, S. E. Nagler, G. E. Granroth, S. Okamoto, G. Alvarez, and D. A. Tennant, Witnessing entanglement in quantum magnets using neutron scattering, *Physical Review B* **103**, 224434 (2021).
- [36] A. Scheie, P. Laurell, A. M. Samarakoon, B. Lake, S. E. Nagler, G. E. Granroth, S. Okamoto, G. Alvarez, and D. A. Tennant, Erratum: Witnessing entanglement in quantum magnets using neutron scattering [Phys. Rev. B 103 , 224434 (2021)], *Physical Review B* **107**, 059902 (2023).
- [37] P. Hauke, M. Heyl, L. Tagliacozzo, and P. Zoller, Measuring multipartite entanglement through dynamic susceptibilities, *Nature Physics* **12**, 778 (2016).
- [38] V. Menon, N. E. Sherman, M. Dupont, A. O. Scheie, D. A. Tennant, and J. E. Moore, Multipartite entanglement in the one-dimensional spin-1/2 Heisenberg antiferromagnet, *Physical Review B* **107**, 054422 (2023).
- [39] P. G. D. Gennes, Inelastic magnetic scattering of neutrons at high temperatures, *Journal of Physics and Chemistry of Solids* **4**, 223 (1958).
- [40] A. Scheie, P. Laurell, B. Lake, S. E. Nagler, M. B. Stone, J.-S. Caux, and D. A. Tennant, Quantum wake dynamics in Heisenberg antiferromagnetic chains, *Nature Communications* **13**, 10.1038/s41467-022-33571-8 (2022).
- [41] V. B. Bulchandani, S. Gopalakrishnan, and E. Ilievski, Superdiffusion in spin chains, *Journal of Statistical Mechanics: Theory and Experiment* **2021**, 084001 (2021).

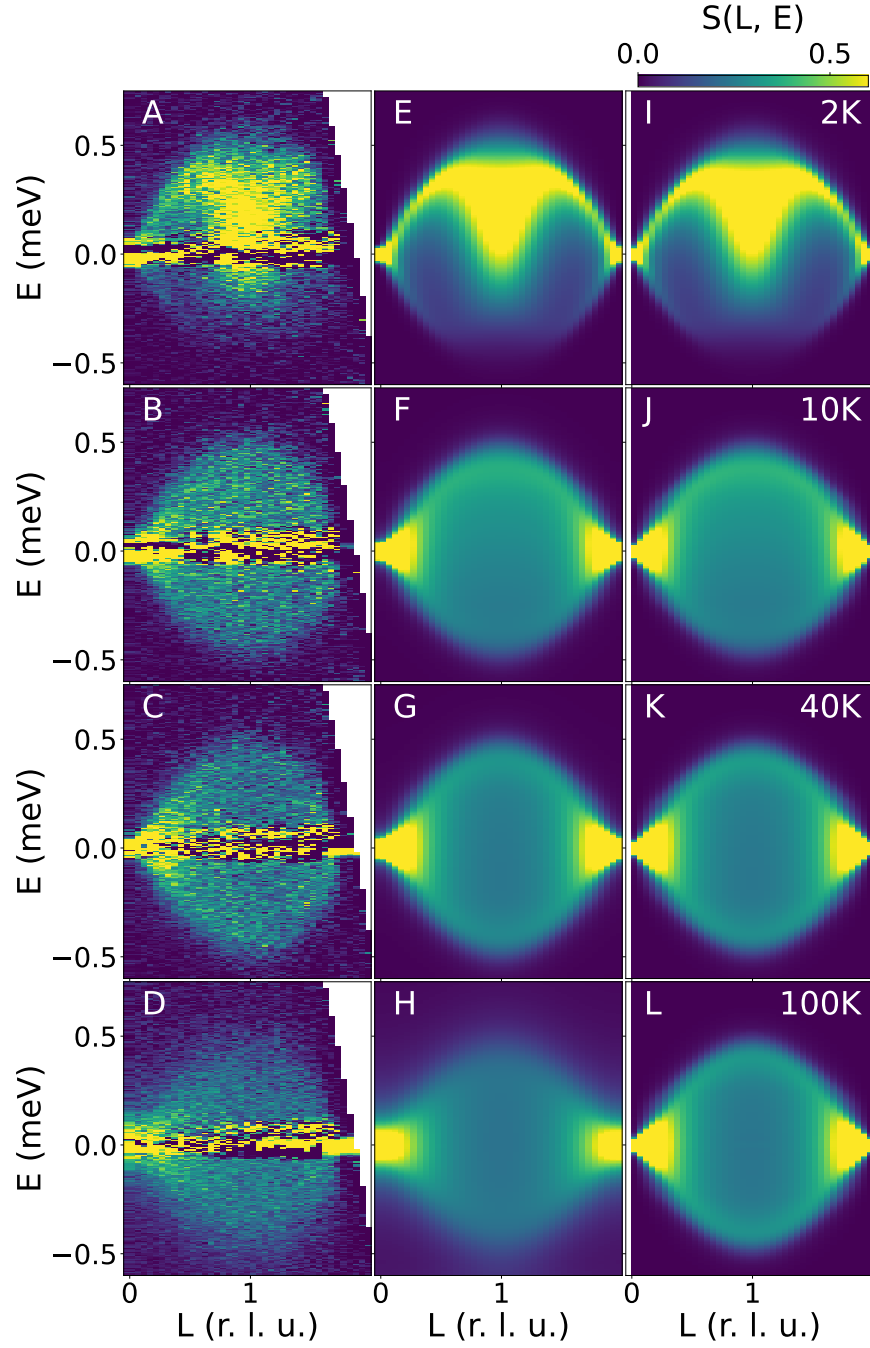


FIG. 1. **The spinon spectra in YbAlO_3 at different temperatures.** (A-D) Color contour maps of the spectral density of the measured neutron scattering intensity at different temperatures. These data are integrated in the dispersionless transverse directions with $K = [-1.0, 1.0]$ and $H = [-0.25, 0.25]$. (E-H) Fits to model constructed from DMRG calculations with Lorentzian broadening accounting for spinon lifetime, as reported in the main text, directly comparable to neutron data. (I-L) Resolution-corrected DMRG calculations without additional Lorentzian broadening accounting for spinon finite lifetime for comparison.

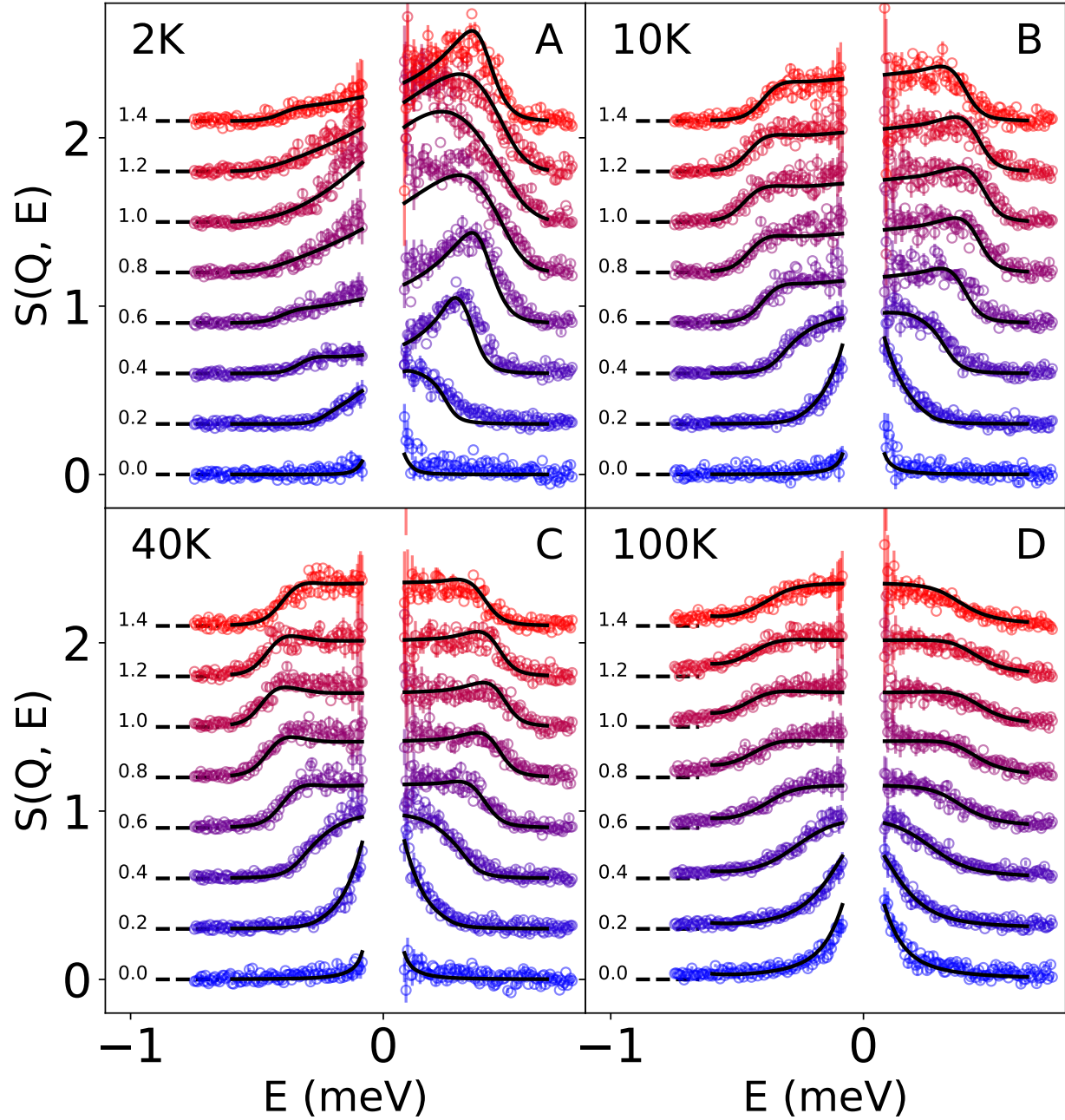


FIG. 2. **Line cuts along the energy axis of our data and fits to our model.** Curves are given an incremental offset for visualization, with dashed leader-lines from each curve signifying the zero of intensity. The labels next to each curve signify the central L value of each line-cut, which are 0.2 r. 1. u. wide. (A) 2 K ($r. \chi^2 = 2.1$); (B) 10 K ($r. \chi^2 = 1.9$); (C) 40 K ($r. \chi^2 = 1.3$); (D) 100 K ($r. \chi^2 = 1.2$)

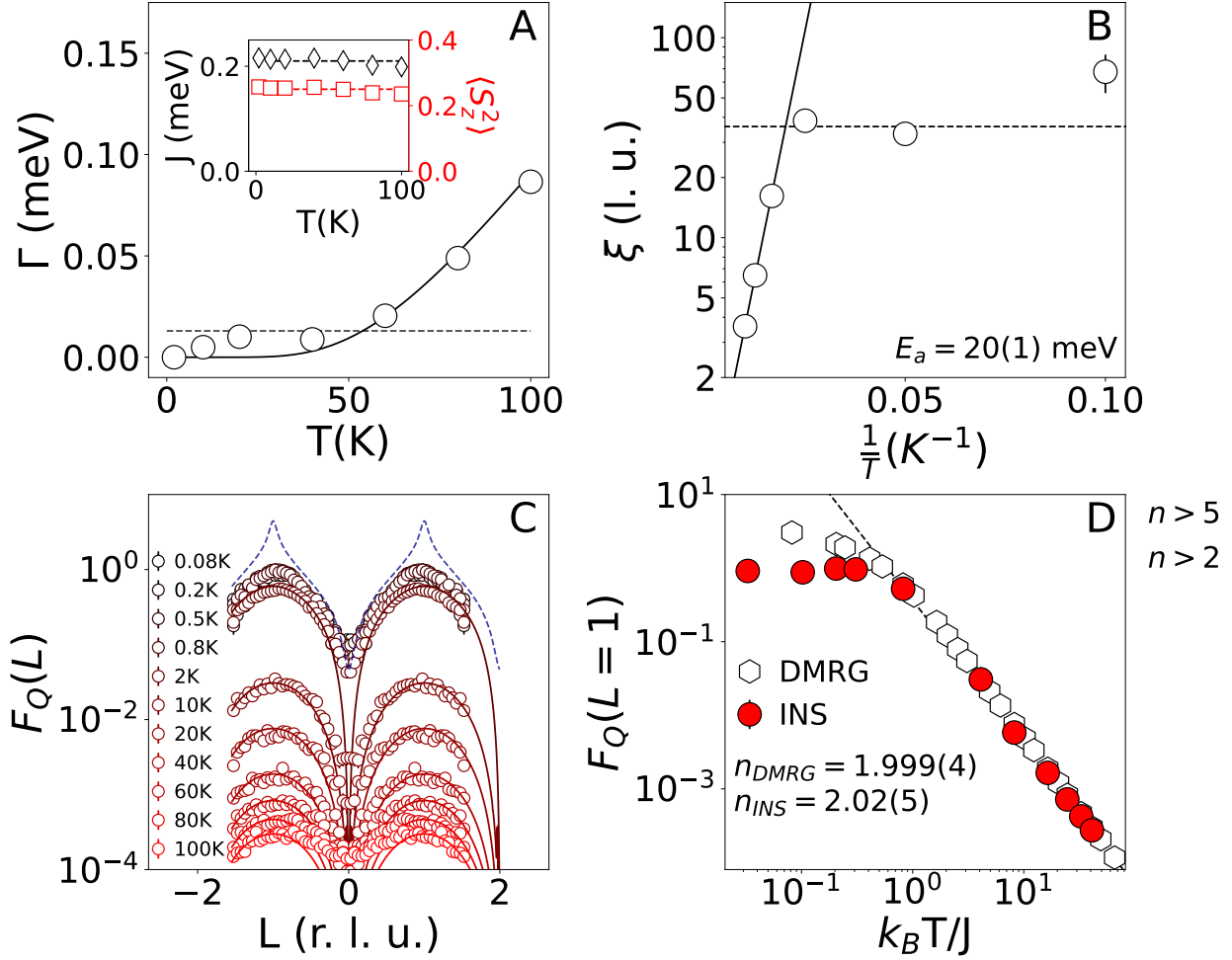


FIG. 3. **Temperature dependence of INS spectral parameters** (A) Life-time broadening parameter as a function of temperature. Dashed line is instrumental resolution HWHM calculated for $E = 0.5$ meV. Solid curve is a fit to Arrhenius-type exponential function as described in the text. (B) Coherence length calculated using the spinon dispersion and extracted lifetime. Solid and dashed lines are asymptotic Arrhenius and resolution-limited behaviors as in (A). (C) F_Q wave-vector dependence at various temperatures. Dashed curve is an approximation to low-temperature limit calculated from DMRG data at 200 mK as described in text. (D) Temperature dependence of maximal quantum Fisher information, $F_Q(L = 1)$. Dashed line is a power-law fit to data for $T \geq 2$ K capturing asymptotic high-temperature behavior.

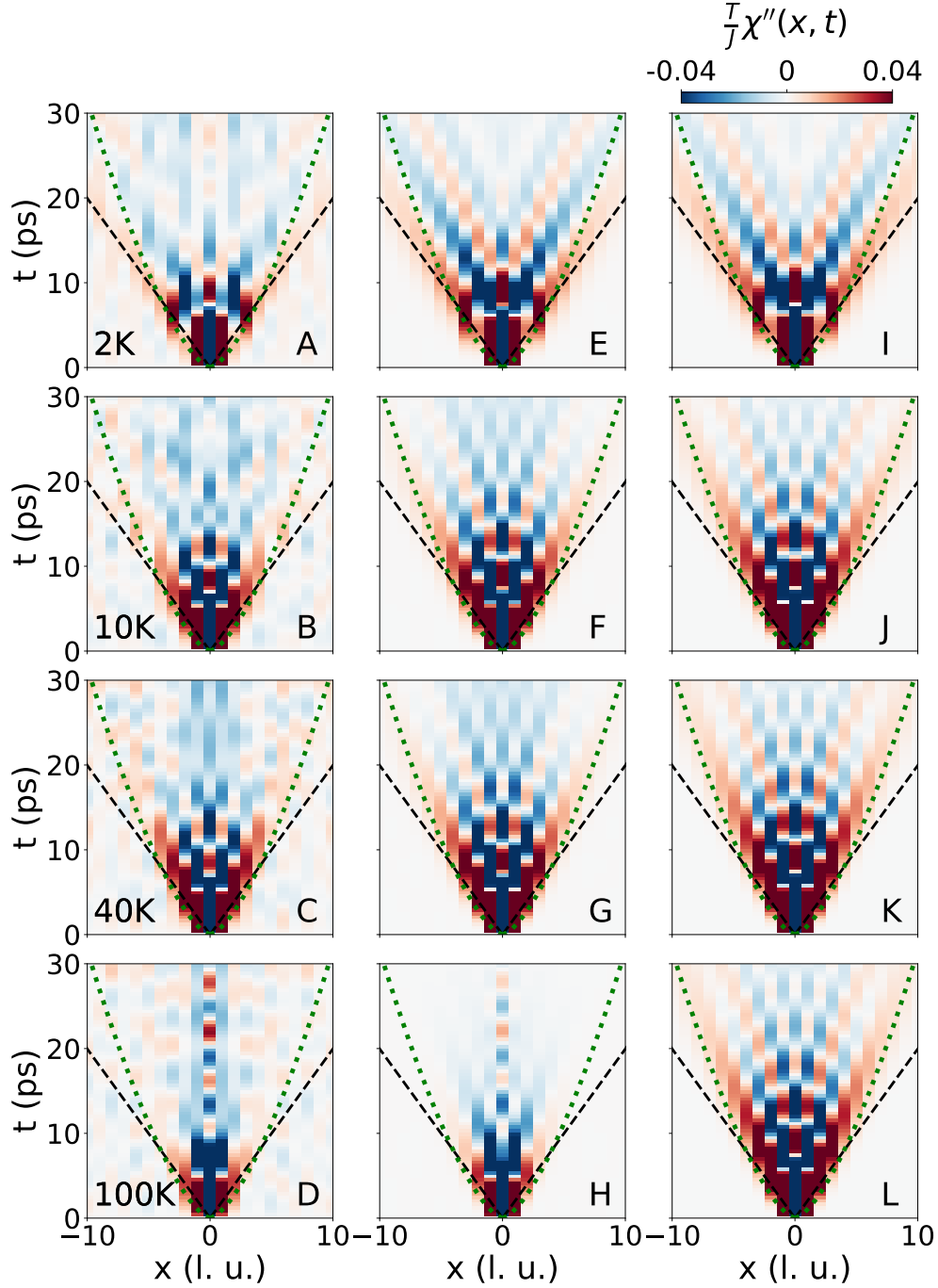


FIG. 4. **Direct-space and time response functions, $\chi''(x, t) = F[\chi''(Q, E)]$, as a function of temperature.** (A-D) Calculated from inelastic neutron scattering spectra; (E-H) Calculated from fits to inelastic neutron data; (I-L) Obtained from DMRG calculations. Dashed black lines mark the edge of the light-cone in the ballistic regime, $t = \frac{x}{2\pi v}$, while dotted green curves highlight the long-time super-diffusive behavior [41] prominent at high temperatures, $t \sim x^{3/2}$.)